PERFORMANCE OF A MAGNETICALLY SUSPENDED FLYWHEEL ENERGY STORAGE SYSTEM

James A. Kirk
Davinder K. Anand
Da-Chen Pang
University of Maryland, College Park, MD, USA

ABSTRACT

A magnetically suspended Open Core Composite Flywheel energy storage systems [OCCF] has been developed for spacecraft applications. The OCCF has been tested to 20,000 RPM where it has a total stored energy of 15.9 WH and an angular momentum of 54.8 N-m-s (40.4 lb-ft-s). Motor current limitations, caused by power losses in the OCCF system, prevented testing to a higher speed. Experimental tests and theoretical analysis suggest that a significant power losse is caused by eddy currents in the magnetic bearing return rings. Our results suggest the losses can be reduced through the use of thin lamination in the magnetic bearing return ring.

INTRODUCTION

In low earth orbit (LEO) satellite applications, spacecraft power is provided by photovoltaic cells and batteries. The batteries store excess photovoltaic power when the satellite sees a 60 minute of sunlight and provide all the power during a 30 minute of darkness. However, electrochemical batteries are known to suffer from limited cycle lifetimes, difficulties in measuring the state of charge, and the inability to test the actual batteries in the spacecraft. To overcome battery shortcomings, the University of Maryland, working with NASA and the Goddard Space Flight center, has developed a magnetically suspended flywheel for energy storage applications [1, 2]. The system shown in Figures 1 and 2 is referred to as an Open Core Composite Flywheel (OCCF) energy storage system.

SYSTEM COMPONENTS

The OCCF system consists of the integration of three key components [3] which are identified in Figure 3. These are:
(1) An interference assembled graphite/epoxy composite flywheel to store the energy.
(2) Two permanent magnet biased active magnetic bearings to suspend the flywheel.
(3) A motor/generator to provide the means of transferring power to and from the system.
In additions, there are a vacuum enclosure producing high vacuum conditions for the system tests on the ground and a display/control panel offering control and data acquisition of the system.
In use the motor accelerates the flywheel to its upper operating speed [75,750 RPM]. When power is required, the motor functions as a generator and the flywheel speed is reduced to its lower operating speed [37,875 RPM]. A brief description of the key components follows.

Composite Flywheel

The composite flywheel is shown in Figures 2 and 3 and consists of two interference assembled graphite/epoxy rings and an inner "metallic" ring for completion of magnetic bearing and motor/generator magnetic paths [2, 4]. The composite flywheel has an inside diameter of 106.7 mm (4.2 in), an outer diameter of 167.9 mm (6.61 in), a height of 228.6 mm (9 in), and a weight of 5.68 Kg (12.5 lb). The composite rings were filament wounded using Toho G40-800 carbon graphite fibers and Shell Epon 826 epoxy resin with a resultant fiber volume fraction of 55%. The two composite rings are assembled together

with an interference fit of 0.1524 mm (0.006 in) and then the "metallic" inner ring is added. Wells [4] calculated that the flywheel will reach a tangential limiting stress at 101,000 RPM [tip speed, 886 m/s]. In order to avoid fatigue failure and to meet 2: 1 operating speed ratio for power conditioning, the flywheel is designed to cycle between 37.5% and 75% of its maximum speed. When the flywheel cycles between the designed speed, 37,875 and 75,750 RPM, it will deliver an energy of 171 WH and a usable specific energy density (SED) of 30.2 WH/Kg.

Magnetic Bearing

The magnetic bearings shown in Figure 4 are designed to allow rotation of the flywheel without any physical contacts [5]. The magnetic bearing has an active feedback control in the radial direction and a passive support in the axial direction. Each magnetic bearing having four permanent magnets and eight electromagnetic coils can independently control two degrees of freedom in motion.

Figure 5 shows a cross section view of the magnetic bearing. A bias flux is generated from the permanent magnets across the air gap as shown in path A and supports the weight of the flywheel. If the flywheel is not centered, the permanent magnets will create a destabilizing force to pull the rotor farther off the center. The control system senses this motion and sends a control current through the EM coils, which results in additional corrective flux as shown in path B. By adding the flux at the small gap side and subtracting the flux at the large gap side, the magnetic bearing produces a net restoring force.

The magnetic bearing has a nominal diameter of 105.66 mm (4.16 in), a height of 98.679 mm (3.885 in), an air gap of 1 mm (0.04 in), and a touchdown gap of 0.127 mm (0.05 in). The permanent magnets are made of Recoma 20, a $SmCo_5$ material. The magnetic cores are made of Carpenter high permeability 49 alloy, a 48% Ni-Fe alloy.

The magnetic bearing has an axial stiffness of 57 N/mm (325 lb/in) and a maximum axial load capability of 71 N (16 lb). This allows the axial drop within 20% of the pole face thickness under 1 g load of the flywheel, 28 N (6.3 lb). In the radial direction, the magnetic bearings are adjusted to a nominal stiffness of 350 N/mm (2000 lb/in) with a load capability of 53 N (12 lb). The magnetic bearing has achieved a DN number of 2.1 million (mm-RPM) at 20,000 RPM.

Motor/Generator

The motor/generator is a 3-phase, 4-pole, permanent magnet DC brushless design [6]. The surface wound armature is mounted in the air gap and attached to the stator laminations. The stator laminations are made of Carpenter HyMu 80 material with a thickness of 0.15 mm (0.006 in). Four Magnet Nd-Fe-Br 32SH permanent magnets are used to generate a large magnetic flux density across the air gap. A commercial DC brushless motor controller, Automation LC-4C, is selected to operate and control the motor/generator. Optical sensors, which have a faster response time and accurate waveform, are used to provide the commutation signals.

The motor/generator has a power rating of 600 W, a voltage constant of 0.02025 V/rad/s, and an overall efficiency of 93%. It has a stator diameter of 89.66 mm (3.53 in) and a height of 64.24 mm (2.53 in) The motor/generator is originally designed with a maximum speed of 80,000 RPM with a supply voltage of 170 V. Because the current limitation of the motor controller [5], the motor/generator can only achieve a maximum speed of 20,000 RPM and a maximum torque of 0.081 N-m (0.0597 lb-ft).

EXPERIMENTAL TESTING & RESULTS

The OCCF system has been tested to 20,000 RPM where the motor controller reached its current limit. At this speed, the flywheel has a total stored energy of 15.9 WH and an angular momentum of 54.8 N-m-s (40.4 lb-ft-s).

Because the OCCF motor limitations were surprising, additional analysis and tests were developed to evaluate the system losses. In particular a spin down test was used to measured the power losses of the OCCF system during operation. The power loss can be calculated knowing the moment of inertia J, the rotating speed ω, and deceleration α of the flywheel. The power loss at this speed is

$$P = J\omega\alpha \qquad (1)$$

Figure 6 shows two testing results of the power loss at various speeds in a vacuum of 0.07 Pa (0.0005 Torr) The power loss is approximately 70 W at 16,000 RPM

SYSTEM LOSSES

Since the OCCF system is magnetically suspended, there are three possible sources of power losses during spinning: windage, hysteresis, and eddy current. The windage losses of the flywheel are due to viscous drag The hysteresis and eddy current losses come from the alternating magnetic field in the magnetic bearing return rings and the motor stator .

Windage Loss in the Vacuum

The aerodynamic flow in a high vacuum condition can be modeled as a free molecular flow. Based on the

theoretical model derived by Pang [5], the total windage loss for the test conditions is less than 0.1 W at 20,000 RPM. Because of its small magnitude, which is about 0.1% of the total power loss, the windage loss in the vacuum is negligible.

Hysteresis Loss

Hysteresis loss occurs when energy is converted into heat because magnetic materials retain magnetism or oppose a change in magnetism. The MIT Electrical Engineering Department Staff [7] suggested that Steinmetz's formula for the symmetrical alternating hysteresis loss is

$$P_{ha} = \eta B_{\max}^{\kappa} f \ (\mathrm{W/m^3}) \qquad (2)$$

where η is the constant coefficient that depends on the magnetic materials, k varies between 1.5 and 2.5 but is generally taken as 1.6, and f is the frequency in Hz. Because our magnetic bearing is a homopolar design, there is mainly an alternating hysteresis loss when the rotor passes the same polarized pole faces. However, our magnetic bearing has a strong DC bias flux density and the above formula cannot be used without further investigation.

Eddy Current Loss and Skin Effect

Eddy currents are developed in the core materials by an induced voltage from a time varying magnetic field. The eddy currents cause an energy loss, I^2R, as heat and they also prevent the magnetic flux from penetrating the center of the core material. The phenomenon that total flux tends to be crowded at the surface of the core materials is known as the skin effect. The skin effect causes reduction in the magnitude and change in phase of the magnetic flux. It also reduces the effective permeability and leads to a larger power loss.

Stoll [8] and Pang [5] have derived a one-dimensional eddy current model with and without skin effect. Assume a semi-infinite plate of thickness t is subjected to a symmetrically sinusoidal magnetic field of a magnitude of H_{max} at a frequency of f Hz. The skin depth or depth of penetration δ is defined as

$$\delta = \sqrt{\rho / \pi \mu f} \qquad (3)$$

where ρ is the electrical resistivity and μ is the permeability of the material.

If the plate thickness equals the skin depth ($t = \delta$), the magnetic field at the center is 98% of the outside surface. The magnetic field drops to 77%, 27%, and 4% of the outside surface as the thickness is 2, 4, and 8 times the skin depth.

When the plate thickness is much larger than the skin depth ($t >> \delta$), the eddy current loss is

$$P_e = \frac{\pi H_{\max} B_{\max} f}{\sqrt{2}} \ (\mathrm{W/m^3}) \qquad (4)$$

Notice that the eddy current loss due to the skin effect is proportional to the product of the maximum magnetic field H_{max}, peak flux density B_{max}, and frequency f. The skin effect of the eddy currents can be easily tested without knowing the normal permeability of the material at various flux densities and frequencies.

The eddy current loss can be greatly reduced if the cores are made from thin laminations of high electrical resistivity materials. When the thickness of the laminations is much less than the skin depth ($t << \delta$), the eddy current loss becomes:

$$P_e = \frac{\pi^2 t^2 B_{\max}^2 f^2}{6\rho} \ (\mathrm{W/m^3}) \qquad (5)$$

Core Loss

When magnetic materials are subjected to an alternating magnetic field, the core loss is the sum of the hysteresis and eddy current losses. The standard method of determining core loss is a magnetization tests. In a DC magnetization test, the cycling frequency of the magnetic field is very low and the energy loss is mainly due to the hysteresis. In the AC magnetization test, the energy loss is the combination of the hysteresis and eddy current. The core loss is usually divided by the mass density of the material and presented as the energy loss per unit mass (W/Kg). Assume the magnetic field and flux density are uniform throughout the cores without the skin effect. The hysteresis and eddy current losses are proportional to the frequency and the square of the frequency of the magnetic field. The core loss also is a function of the peak flux density, so

$$P_c = a B_{\max}^{k} f + b B_{\max}^{n} f^2 \ (\mathrm{W/Kg}) \qquad (6)$$

where a and b are constant coefficients of hysteresis and eddy current losses. The k is approximately 1.6 and n is equal to 2.

Magnetization Test

Magnetization tests were conducted on the magnetic bearing return rings to study the core loss of non-laminated 48% Ni-Fe alloy. The testing results will compare to the experimental data from the manufacturer's laminated specimens [9].

The C-shape return ring has an outside diameter of 118.9 mm (4.68 in), an inside diameter of 106.7 mm (4.2 in), and a minimum thickness of 3.05 mm (0.12 in). The return rings were tested using a LDJ 3500H hysteresigraph system. In the DC tests, the rings are tested at two peak magnetic fields, 159 and 1592 A/m (2 and 20 Oe). In the AC tests, the rings are tested

under three maximum flux density levels, 0.6, 0.8, and 1 Tesla at frequencies of 60 and 400 Hz. The levels of the flux densities are chosen to simulate the real flux density distribution of the magnetic bearings.
The manufacturer's ring specimens have an outside diameter of 38.1 mm (1.5 in), an inside diameter of 25.4 mm (1 in), and a thickness of 0.36 mm (0.014 in). The available data for comparison are the DC magnetic property at the peak magnetic field of 159 A/m (2 Oe) and AC magnetic properties of three magnetic flux density levels, 0.2, 0.4, and 0.8 Tesla at frequencies of 60 and 400 Hz.
Table 1 summarizes the magnetization test results of the return rings and the manufacturer's specimens. The magnetic properties are almost identical in the DC tests but vastly different in the AC tests. For example, the return ring requires a maximum magnetic field of 614 A/m to achieve the maximum flux density of 0.8 Tesla at 60 Hz, but the manufacturer's specimens need only 11.7 A/m. The core loss is 9 W/Kg for the return ring but only 0.163 W/Kg for manufacturer's specimens. The core loss of the return ring is about 40 to 100 times larger than the manufacturer's specimens at the similar conditions. This large difference suggests that the power loss in the OCCF system during the spin-down test are caused by the magnetic losses.

Analysis of Losses in Magnetic Cores
In order to reduce the core loss, the knowledge of relative magnitudes of the hysteresis and eddy current losses is very important. If the hysteresis loss is dominant, the only option is to choose the magnetic material with a small hysteresis loop. If the eddy current loss becomes dominant, the option is to use thin laminations and/or high resistivity and low loss materials. Although both losses can be reduced by using low peak flux density and cycling frequencies, it is not always feasible in magnetic applications.

Core Loss of Laminated Specimens. For the manufacturer's laminated specimens, the magnetic field is uniform throughout the cores and there is no skin effect. The hysteresis and eddy current components can be separated using the core losses tested at two frequencies of 60 and 400 Hz. By applying equation (6), the coefficients k and n are found to be 1.587 and 1.957. If the k and n are 1.6 and 2, the formula for core loss estimation becomes

$$P_c = 2.24\times10^{-3} B_{max}^{1.6} f + 3.09\times10^{-5} B_{max}^{2} f^{2} \quad (7)$$

The errors for the core loss estimations are within 1% at 60 Hz and 9% at 400 Hz.
The results show that the formulas for hysteresis and eddy current losses are fairly accurate for the laminated specimens. The hysteresis loss is the major loss at 60 Hz but the eddy current loss becomes dominant at 400 Hz. The eddy current loss accounts 85% of the core loss at the flux density of 0.8 Tesla with the frequency of 400 Hz.

Core Loss of Non-laminated Return Rings. The core loss of the non-laminated return rings is mainly caused by the skin effect of the eddy currents. From the experimental data, the hysteresis losses account less than 2% of the AC core losses at both 60 and 400 Hz. The empirical formula for eddy current loss per unit mass can be expressed as

$$P_e = \frac{\xi H_{max} B_{max} f}{d_m} \text{ (W/Kg)} \quad (8)$$

where ξ is the shape factor (which is $\pi/\sqrt{2}$ or 2.22 for one-dimensional model), and d_m is 8249 Kg/m^3 for 48% Ni-Fe alloy.
Using the experimental data, the shape factor ξ for the return rings is calculated to be 2.505 with an error of less than 3%. The result also shows that the core loss for the C-shaped return ring is 14% more than one-dimensional model.
Although the testing results are based on normal (major) hysteresis loops of the magnetic materials, the cores are subjected to biased (minor) hysteresis loops in our magnetic bearings. The magnetization tests reveal that the eddy current loss is the major power loss in the spin-down tests. For an accurate analysis of the core loss, there is a need for the magnetization testing of minor hysteresis loops that resemble the real conditions in the magnetic bearings.

Reduction of Core Loss. To eliminate skin effect in the magnetic cores, the lamination thickness should be designed less than twice the skin depth. Assume the 48% Ni-Fe alloy has a AC relative permeability of 100,000 and electrical resistivity of 480 μΩ-mm. Because of 4-pole magnetic bearing design, a rotating speed of 75,750 RPM will generate a cycling magnetic field of 5,050 Hz. By applying equation (2), the skin depth is found to be 0.0155 mm (0.00061 in) at the upper operating speed of 75,750 RPM. Therefore, a lamination thickness of 0.0254 mm (0.001 in) is suggested. The return rings will be laminated as a cylindrical shape in the axial direction.

CONCLUSIONS

The Open Core Composite Flywheel system has been successfully tested to 20,000 RPM where the total stored energy is 15.9 WH and the angular momentum is 54.8 N-m-s (40.4 lb-ft-s). The OCCF system was unable to reach a higher speed because power losses

exceeded the power capability of the motor controller. Experimental magnetization tests and theoretical analysis have shown the power loss is due to the skin effect of the eddy currents in the non-laminated return rings. To reduce eddy current loss the magnetic return ring must be laminated to an effective thickness of 0.0254 mm (0.001 inch).

TABLE 1: Magnetization Testing Results

Specimen	f (Hz)	Bmax (T)	Hmax (A/m)	P (W-s/Kg)
Return Ring	DC	1.27	159	0.0058
Return Ring	DC	1.57	1592	0.0128
Manufact.	DC	1.26	159	N/A
Specimen	f (Hz)	Bmax (T)	Hmax (A/m)	Pc (W/Kg)
Return Ring	60	0.60	354	3.98
Return Ring	60	0.81	614	9.00
Return Ring	60	1.01	949	17.40
Return Ring	400	0.61	1920	143.00
Return Ring	400	0.81	3215	316.08
Return Ring	400	1.01	4760	581.50
Manufact.	60	0.20	4.19	0.015
Manufact.	60	0.40	6.55	0.049
Manufact.	60	0.80	11.72	0.163
Manufact.	400	0.20	11.97	0.282
Manufact.	400	0.40	20.37	0.914
Manufact.	400	0.80	54.76	3.860

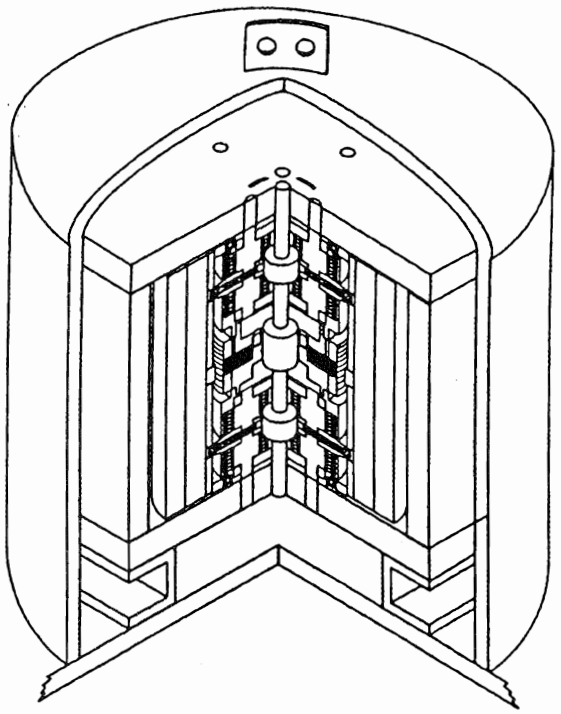

FIGURE 1: The OCCF Energy Storage System

REFERENCE

1. Anand, D. K., Kirk, J. A., Zmood, R. B., Pang, D., and Lashley, C., "Final Prototype of Magnetically Suspended Flywheel Energy Storage System," Proceedings of the 26th Intersociety Energy Conversion Engineering Conference, August 4-9, 1991, Boston, Massachusetts, pgs. 203-208.
2. Wells, S. P., Pang, D., and Kirk, J. A., "Testing and Improvements in a Magnetically Suspended Composite Flywheel Energy Storage System", Proceedings of the 2nd International Symposium on Magnetic Suspension Technology, August 11-13, 1993, Seattle, Washington, pgs. 19 - 34.
3. Kirk, J. A., Anand, D. K., "The Magnetically Suspended Flywheel as an Energy Storage Device", NASA Pub. No. 2484, "Space Electrochemical Research and Technology (SERT)", pgs. 137-146, 1987.
4. Wells, S. P., "Manufacture and Testing of a Composite Material Flywheel for Energy Storage", Master Thesis, University of Maryland, College Park, 1993.
5. Pang, D., "Magnetic Bearing System Design for Enhanced Stability", Ph.D. Dissertation, University of Maryland, College Park, 1994.
6. Lashley, C., Anand, D. K., Kirk, J. A., and Zmood, R. B., "Development of a High Efficiency Motor/Generator for Flywheel Energy Storage," Proceedings of the 26th Intersociety Energy Conversion Engineering Conference, August 4-9, 1991, Boston, Massachusetts, pgs. 221-226.
7. MIT Department of Electrical Engineering Staff, "Magnetic Circuit and Transformer", John Wiley & Sons, Inc., New York, NY, 1943.
8. Stoll, R. L., "The Analysis of Eddy Currents", Clarendon Press, Oxford, Great Britain, 1974.
9. Carpenter Technology Corporation, Internal Document, Reading, PA.

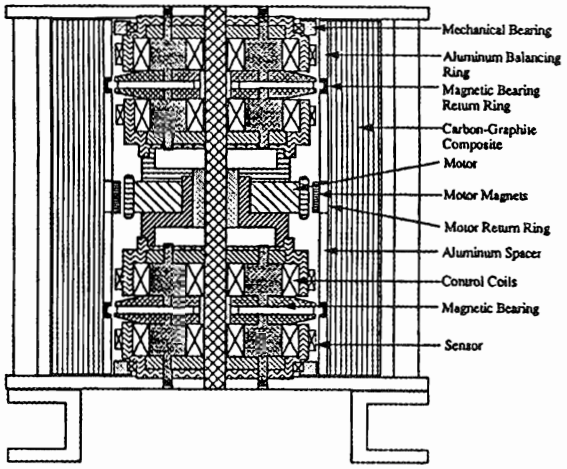

FIGURE 2: Cross section of the OCCF Energy Storage System

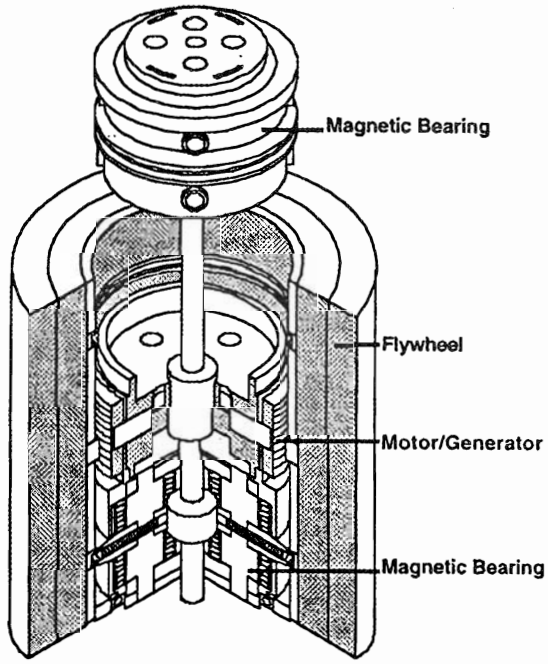

FIGURE 3: Key components of the OCCF

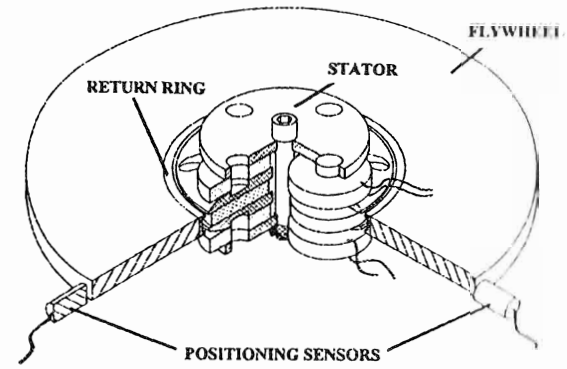

FIGURE 4: Pancake permanent magnet biased active magnetic bearing for the OCCF

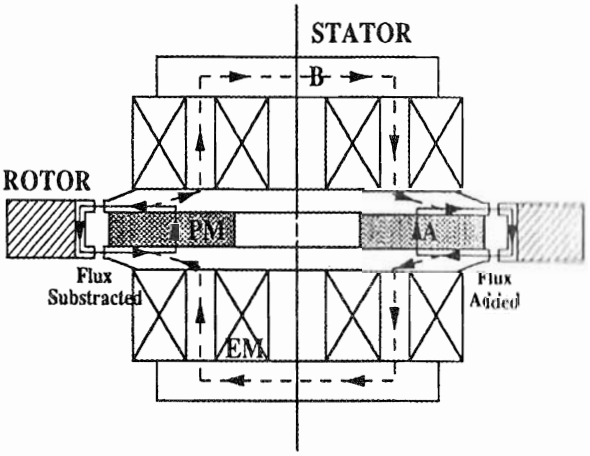

FIGURE 5: Flux path for the OCCF magnetic bearing

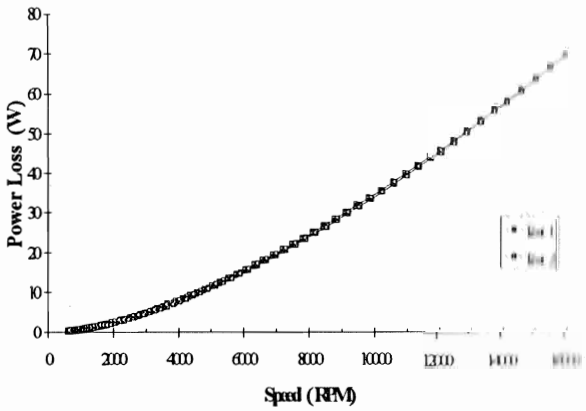

FIGURE 6: Measured power loss of the OCCF in a Vacuum of 0.07 Pa (5E-4 torr)